


# Liquid repellency enhancement through flexible microstructures

## Journal Article

### Author(s):

Hu, Songtao; [Cao, Xiaobao](#) ; Reddyhoff, Tom; Puhan, Debashis; Vladescu, Sorin-Cristian; Wang, Jing; Shi, Xi; Peng, Zhike; de Mello, Andrew J.; Dini, Daniele

### Publication date:

2020-08-05

### Permanent link:

<https://doi.org/10.3929/ethz-b-000438558>

### Rights / license:

[Creative Commons Attribution-NonCommercial 4.0 International](#)

### Originally published in:

Science Advances 6(32), <https://doi.org/10.1126/sciadv.aba9721>

## MATERIALS SCIENCE

## Liquid repellency enhancement through flexible microstructures

Songtao Hu<sup>1\*</sup>, Xiaobao Cao<sup>2\*</sup>, Tom Reddyhoff<sup>3</sup>, Debashis Puhon<sup>3</sup>, Sorin-Cristian Vladescu<sup>3</sup>, Jing Wang<sup>4,5</sup>, Xi Shi<sup>1†</sup>, Zhike Peng<sup>1†</sup>, Andrew J. deMello<sup>2</sup>, Daniele Dini<sup>3</sup>

Artificial liquid-repellent surfaces have attracted substantial scientific and industrial attention with a focus on creating functional topological features; however, the role of the underlying structures has been overlooked. Recent developments in micro-nanofabrication allow us now to construct a skin-muscle type system combining interfacial liquid repellence atop a mechanically functional structure. Specifically, we design surfaces comprising bioinspired, mushroom-like repelling heads and spring-like flexible supports, which are realized by three-dimensional direct laser lithography. The flexible supports elevate liquid repellency by resisting droplet impalement and reducing contact time. This, previously unknown, use of spring-like flexible supports to enhance liquid repellency provides an excellent level of control over droplet manipulation. Moreover, this extends repellent microstructure research from statics to dynamics and is envisioned to yield functionalities and possibilities by linking functional surfaces and mechanical metamaterials.

## INTRODUCTION

Artificial liquid-repellent surfaces have recently attracted substantial attention because the interplay between liquid droplets and solid interfaces is of great importance to many scientific principles and technological applications from self-cleaning, anti-icing, antireflection, water harvesting, and bioanalysis to droplet manipulation (1–6). For synthetic systems, researchers are interested in mimicking morphological and chemical attributes of natural surfaces, which fulfill their evolved functions to environmental physicochemical reactions, following a common pathway in biomimetics (7). The most well-known natural inspiration is the lotus effect that exhibits water-proofing performance via a flawless combination of hierarchical morphology and wax-based chemical modification. However, traditional hierarchical structures, even if embellished with low-surface energy coatings, still trouble about a sustained Cassie state and strong omni-repellency. To improve upon the lotus effect, a mushroom-like topology has been discovered from the cuticles, with which springtails are able to prevent both water and low-surface tension organic solvents so as to guarantee dermal respiration in aqueous environments, thereby becoming the most widespread arthropods on Earth with extreme habitats including Antarctic and the Arctic (8). This springtail-inspired topology has developed into a classic geometry with mushroom-like heads atop pillar-like supports (9–18).

So far, the emphasis of mushroom-like micro/nanointerfacial structures has been on optimizing head design (e.g., singly, doubly, or triply reentrant topology) to impart enhanced liquid repellency. Some researchers have reported interconnected or stratified underlying supports to improve mechanical robustness (13, 18) and an undulated substrate with micro wrinkles to attain extreme kinetic repellency to impinging droplets (16). Yet, these studies were trapped by rigid settings. Recently, inspired by a broad palette of surfaces in

nature (e.g., leaves and wings), flexible surfaces made of soft materials and arranged as simply supported or cantilever beams have been proposed to improve kinetic repellency, particularly the contact time reduction of impacting events for anti-icing (19–23). Since this milestone, studies on liquid repellency have transferred from conventional statics to dynamics, thus broadening the way of wettability tuning. However, because the entirety of these flexible surfaces oscillates at impact, repellence enhancement is strongly dependent on the impacting position. In addition, the requirement of whole-surface oscillation limits the applicability of flexible repellent surfaces. For instance, the oscillation of an anti-icing flexible surface results in aircraft skin deformation that weakens aerodynamic performance.

Here, we present a liquid repellence enhancement through flexible microstructures, i.e., mature mushroom-like repelling heads (9–18) atop spring-like flexible supports (24). Our design is of great technological interest, because it bridges the gap between the two research realms of functional surfaces and mechanical materials, thereby constructing a “skin-muscle” system where the top interfacial structures behave as the skin to receive and respond to surrounding stimulus, while the underlying flexible supports play the muscle role to tune mechanical properties. Using three-dimensional (3D) direct laser lithography micro-nanofabrication, we realize the mushroom-spring design and prove its elevation on kinetic repellency to droplet intrusion in terms of droplet impalement resistance and contact time reduction. We believe this study to be the first demonstration of spring-like flexible supports to promote the liquid repellence of mushroom-like interfacial structures, providing an unprecedented level of control over droplet repellency and manipulation and extending macro/nanostructures’ liquid repellency from statics to dynamics. Also, this is expected to trigger a window of opportunity for more functionalities and possibilities by linking functional surfaces and mechanical metamaterials (25).

## RESULTS

## Design and fabrication

To realize our mushroom-spring design, we conducted direct laser lithography based on a two-photon polymerization on Photonic Professional System (Nanoscribe GmbH, Germany) because it is the

Copyright © 2020  
The Authors, some  
rights reserved;  
exclusive licensee  
American Association  
for the Advancement  
of Science. No claim to  
original U.S. Government  
Works. Distributed  
under a Creative  
Commons Attribution  
NonCommercial  
License 4.0 (CC BY-NC).

<sup>1</sup>State Key Laboratory of Mechanical System and Vibration, Shanghai Jiao Tong University, Shanghai 200240, China. <sup>2</sup>Department of Chemistry and Applied Biosciences, ETH Zurich, Zurich 8093, Switzerland. <sup>3</sup>Department of Mechanical Engineering, Imperial College London, London SW7 2AZ, UK. <sup>4</sup>Institute of Environmental Engineering, ETH Zurich, Zurich 8093, Switzerland. <sup>5</sup>Laboratory for Advanced Analytical Technologies, Empa, Dübendorf 8600, Switzerland.

\*These authors contributed equally to this work.

†Corresponding author. Email: xishi@sjtu.edu.cn (X.S.); z.peng@sjtu.edu.cn (Z.P.)

most precise rapid prototyping technology to tailor 3D structures on the micro-nanoscale. This up-to-date printing technology has been successfully applied to optics, photonics, biology, mechanical metamaterials, etc. and has also provided a broad avenue to shed light on wettability research (17, 18, 26–30). Three mushroom-spring flexible surfaces (see S1, S2, and S3 in Fig. 1A) were modeled in SolidWorks (Dassault Systèmes, France) as well as a traditional mushroom-pillar rigid surface (P) as a reference. On each designed surface, mushroom-spring or mushroom-pillar structural elements were prescribed in a rectangular array with a pitch  $p$  of 90  $\mu\text{m}$ . The height (or free height) of the supporting pillars (or springs)  $h_3$  was set to 100  $\mu\text{m}$ , and the diameter (or outer diameter)  $d_2$  was set to 30  $\mu\text{m}$ . The three mushroom-spring flexible surfaces had the same coil diameter  $d_3$  (5  $\mu\text{m}$ ) but different numbers of active coils (2, 3, and 4 on S1, S2, and S3, respectively). With regard to the mushroom-like waterproofing head, a doubly reentrant topology (see inset in Fig. 1A) inspired by springtail cuticles was used by setting  $d_1$  to 60  $\mu\text{m}$ ,  $h_1$  to 2  $\mu\text{m}$ ,  $h_2$  to 4  $\mu\text{m}$ , and  $w$  to 1  $\mu\text{m}$ . Designs of these structures were converted into a stereolithography format and input into the Nanoscribe system to be fabricated with IP-S photoresist (Nanoscribe GmbH, Germany) on an ITO (Indium Tin Oxide)-coated fused silica. The resulting fabrication was then coated with a low-surface energy 1H,1H,2H,2H-perfluorooctyltrichlorosilane layer via chemical vapor deposition (see Fig. 1B). With such a large aspect ratio, the mushroom-spring flexible surfaces encountered structural instability owing to

the stress concentration induced during sample postprocessing. One alternative was to reduce the height of the supporting structures (see fig. S1). However, a shorter structural height left little compression space, thereby making the flexible springs behave as rigid pillars.

We further proposed a trampoline-inspired solution with vertical springs to support mushroom-like heads and horizontal springs to link adjacent mushroom-like heads (see SS1, SS2, and SS3 in Fig. 1C). When one head oscillated with the aid of its vertical spring, its relative independence on movement can be guaranteed by the flexibility of the horizontal springs (see fig. S8). For these horizontal springs, the coil diameter and active coil number were set to 5  $\mu\text{m}$  and 3, respectively. The fabrication in Fig. 1D indicated our processing approach as an effective avenue to integrate bioinspired interfacial structures with flexible mechanical supports. Notably, each trampoline-inspired surface was purposely designed as a matrix consisting of uniform units, each comprising  $9 \times 9$  structural elements. The reason for such a matrix design was related to the finite size of scanning blocks (280  $\mu\text{m}$  by 280  $\mu\text{m}$ ) on the Nanoscribe system combined with the coincident difficulty in processing horizontally impeding springs between adjacent blocks (see fig. S2). Also, the corresponding pillar case (see PS in Fig. 1, C and D) was included as a reference.

### Impalement resistance

The mushroom-pillar and mushroom-spring surfaces exhibited an excellent anti-penetrating capacity to static water droplets with contact

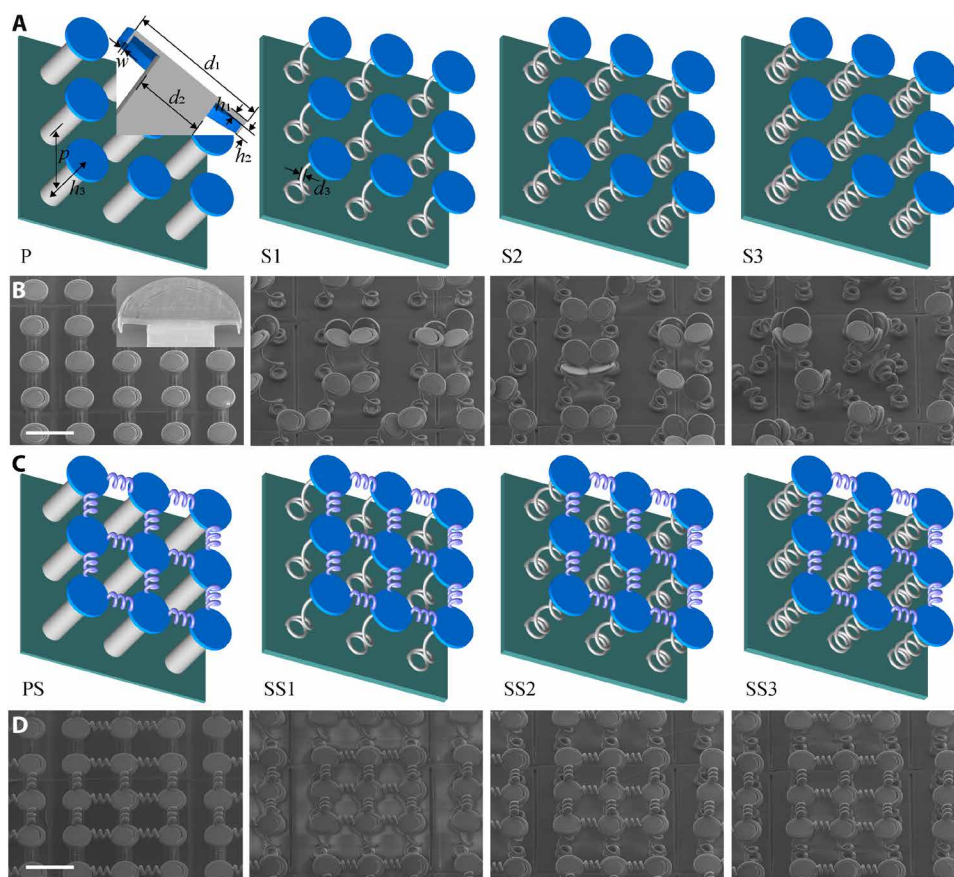


**Fig. 1. Mushroom-spring and mushroom-pillar surfaces.** (A and B) Design and fabrication of mushroom-spring flexible surfaces S1, S2, and S3, as well as a mushroom-pillar rigid reference P. (C and D) Design and fabrication of mushroom-spring flexible surfaces SS1, SS2, and SS3, as well as a mushroom-pillar rigid reference PS with horizontal springs to link adjacent heads. Scale bars, 100  $\mu\text{m}$ .

angle, respectively, reaching 151.0°, 149.0°, 150.5°, 149.5°, 157.4°, 156.6°, 156.3°, and 156.7° on P, S1, S2, S3, SS1, SS2, and SS3 (see fig. S3A) in comparison to the value of 67.2° on a smooth plane made of the same photoresist (30), thereby demonstrating a drastic transformation in repellency from inherent hydrophilicity to structural hydrophobicity, powered by the combination of bioinspired topology with low-surface energy coatings. In contrast to the Wenzel state, under the Cassie state, the droplet no longer conformed to the substrate but rested atop the heads simultaneously generating air pockets beneath them, which connect to atmosphere so that the droplet was suspended solely by surface tension regardless of extra pressure generated from the trapped air (12). The repelling contribution of bioinspired topology consisted of the handpicked mushroom-like heads (9–18) and the Fakir effect of large aspect ratio supports (31). Horizontal springs improved the contact angle from ~150° to ~156° because they increased the surface roughness and reduced the fraction of solid-liquid interface. Also noteworthy was the observation that the contact angles decreased mildly when the underlying supports changed from pillars to springs, which seemed to imply a weakened static repellence due to the flexible modification. However, it should be noted that the contact angle is a macroscopic index based on a specified baseline (see fig. S3B). A partial compression of spring-like supports will spontaneously generate a reduced contact angle value so as to underestimate the real static repellency.

The importance of flexible support modification combined with mushroom-like microstructures can be inspected for the kinetic resistance to impinging droplets. We therefore conducted impacting tests to analyze the spreading, retracting, and post-retraction behaviors of water droplets under different impacting velocities, as recorded in movie S1. Figure 2A summarized the post-retraction behaviors translating from depositing (DEP), rebounding (REB) to pinning (PIN) along with an increased  $We$  (also listed in table S1), which was nondimensionalized as  $D_0\rho V_0^2/\sigma$  to quantify the ratio between inertial and capillary forces. Here,  $D_0$  and  $V_0$  are the diameter and impacting velocity of a droplet in flight before the contact instant, respectively; and  $\rho$  and  $\sigma$  are the density and surface tension of a droplet, respectively. Some exemplary snapshots for the case P at  $We \sim 1.08, 2.42,$  and  $13.20$  were provided in Fig. 2B to visualize the DEP, REB, and PIN motions over time. For the defined DEP behavior, the impinging droplet spread to the maximum diameter  $D_{max}$  and then

retracted; as the impacting energy was low enough to be exhausted in the spreading and retracting phases, the droplet lastly beaded up on the mushroom-like heads, yielding the Cassie state. When the impacting energy increased (denoted by the increased  $We$  value), the REB behavior inherited the place of the DEP one, exhibiting an effective kinetic resistance to impacting events. Note that, in this study, the defined REB included full and partial bouncing (see fig. S4). With regard to the PIN definition, because of an extremely high pressure arising from a high impacting velocity, the droplet impaled the defense of mushroom-like heads so as to enter the Wenzel state.

At the start of the  $We$  increase (see Fig. 2A and table S1), the mushroom-pillar rigid surface (P) was easier to render a bouncing response to impinging droplets than the mushroom-spring flexible surfaces (S1, S2, and S3), indicating an extra energy loss in the compression and extension phases of the springs. This phenomenon can be also observed in the trampoline series (PS versus SS1, SS2, and SS3). When  $We$  increased to  $\sim 10.51$  and  $\sim 11.18$ , the bouncing behavior began to disappear on the mushroom-spring surfaces (S1, S2, and S3) and was substituted by a pinning action. In contrast, the mushroom-pillar surface (P) still maintained water repellency and only transformed into a pinning consequence when the value of  $We$  continued to rise over  $\sim 13.20$ . However, it is not reasonable to speculate that spring-like flexible supports will weaken the droplet impalement resistance in comparison to pillar-like rigid supports because of the existence of structural instability on S1, S2, and S3. A pinning motion started to appear on the trampoline-inspired mushroom-spring surfaces (SS1, SS2, and SS3) when the value of  $We$  increased to  $\sim 19.93$ . This indicates a 50.98% enhancement (i.e., the breakthrough limit increased from  $\sim 13.20$  to  $\sim 19.93$ ) in comparison to the mushroom-pillar surface (P), which is attributed to the reduction of relative impacting velocity and force arising from the downward movement of flexible supports (19–23). However, because of the repellency improvement afforded by the additional horizontal springs (i.e., the breakthrough limit was  $\sim 17.24$  on the surface PS), the enhancement provided solely by flexible supports should be quantified as 15.60%. It appears that the enhancement facilitated by the oscillation of flexible microstructures is smaller than that facilitated by the entire oscillation of flexible surfaces (19–23), which can be ascribed to the constrained oscillation amplitude. More precisely, the oscillation amplitude of report flexible surfaces was more than  $200 \mu\text{m}$  (19–23), which is two times larger than the free height of our

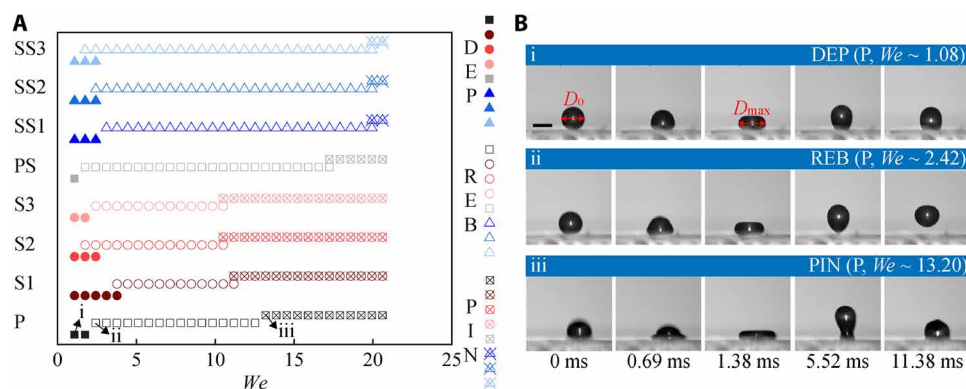


**Fig. 2. Post-retraction behavior of droplets impacting mushroom-spring and mushroom-pillar surfaces.** (A) Post-retraction behaviors, including depositing (DEP), rebounding (REB), and pinning (PIN), as a function of  $We$ . (B) Snapshots exemplarily provided to visualize different post-retraction behaviors over time. Scale bar, 1 mm. Photo credit: S. Hu, Shanghai Jiao Tong University.

flexible microstructures. In addition, the mushroom-spring flexible surfaces in the same group (S1, S2, and S3; SS1, SS2, and SS3) reached the pinning phase at the same  $We$ , indicating a complete compression on each flexible surface, again highlighted the confined oscillation space.

### Spreading performance

Figure 3A presented the maximum spreading factor  $D_{\max}/D_0$  as a function of  $We$ . The mushroom-spring flexible surfaces exhibited a smaller maximum spreading factor than the mushroom-pillar rigid surfaces at the same  $We$ , in consistent with the findings in previous works (19–23) via different mechanisms. In previous studies, the natural frequency of oscillation of the surface was smaller than that of the spreading droplet, indicating a downward movement of the flexible surface across the entire spreading phase of the droplet. The downward movement of the surface decreased the relative impact velocity and force, resulting in a reduced value of  $D_{\max}/D_0$ . When the surface achieved its maximum deformation before the droplet reached its maximum spread, the elastic potential energy returned to the droplet and participated in the spreading motion. Although there was an energy consumption in the surface oscillation, the difference in  $D_{\max}/D_0$  between the flexible and rigid cases was not obvious. Hence, the difference we observe in  $D_{\max}/D_0$  can be mainly attributed to the viscoelastic breaking that occurs in soft materials (32). The viscoelastic breaking dissipates energy in the contact line due to local compliance on a soft surface, which inspires us to consider the frequency relation between flexible microstructures and impinging droplets. Namely, even if the natural frequency of the microstructures is greater than that of the spreading droplet, the flexibility-based difference of  $D_{\max}/D_0$  may still be maintained because of the different working time for flexible microstructures. More precisely, when the center microstructure beneath the spreading droplet has reached a complete compression, the microstructures beyond the outermost rim of the droplet are still in their uncompressed, equilibrium condition, and the others are partially compressed.

To further explore how a mushroom-spring combination can affect the spreading behavior of impinging droplets, we established a theoretical spreading model based on energy conservation to estimate the work done  $W$  in spreading out to maximum diameter, which includes both rigid and flexible cases (see Fig. 3B that was clearly modeled in section S3), rendered as

$$W = \begin{cases} W_1 + W_2 & \text{rigid case} \\ W_1 + W_2 + W_3 & \text{flexible case} \end{cases} \quad (1)$$

$$W_1 = \frac{\pi\rho D_0^3 V_0^2}{12} + \pi\sigma D_0^2 - \frac{\pi\sigma D_{\max}^2(1 - \cos\theta)}{4}$$

$$W_2 = \frac{\pi\rho g D_0^3}{6} \left( \frac{D_0}{2} - \frac{D_0^3}{3D_{\max}^2} \right)$$

$$W_3 = \frac{\pi\rho g D_0^3}{6} (h_3 - h_{3,c}) - \frac{nk(h_3 - h_{3,c})^2}{2}$$

In this model,  $\theta$  is the apparent contact angle,  $g$  is the gravitational acceleration,  $n$  is the number of compressed springs,  $k$  is the spring stiffness, and  $h_{3,c}$  is the compressed spring height. Using this model, we calculated the value of  $W$  and then depicted in Fig. 3C. Of note, in the flexible case, the spring stiffness  $k$  and the compressed height  $h_{3,c}$  were calculated through a load-displacement mechanics simulation using COMSOL Multiphysics (COMSOL Inc., UK) (see fig. S7). In comparison to the mushroom-pillar rigid surfaces, the spreading droplets dissipated more energy on the mushroom-spring flexible surfaces, which can be used to verify the reduced restitution coefficient in the next section. Looking at the mushroom-spring flexible surfaces (see fig. S6B), the rigid model overstated the energy dissipation during the spreading phase in comparison to the flexible model. It appeared that the overstated deviation was sufficiently small to be neglected. However, the applied normal load in the simulation was underestimated referring to a theoretical expression by  $0.25 \pi\rho D_0^2 V_0^2$  (33). On the basis of the underestimated normal load, the resulting compressed height  $h_{3,c}$  was only around 10 to 13  $\mu\text{m}$  when  $We$  arrived at the maximum value of  $\sim 20.61$  (see fig. S7), which were in contrast to the full compression conclusion drawn from the above analysis of post-retraction behaviors.

### Restitution coefficient

Figure 4A presented the restitution coefficient  $H_{\max}/H$  used to quantify the remaining kinetic energy of the droplets after lifting off the surfaces regardless of any mass loss due to partial bouncing. Here,  $H$  is the height to release the droplet, and  $H_{\max}$  is the maximum bouncing height that is defined as the distance from the topside of mushroom-like heads to the lowermost rim of the droplet. The restitution coefficient of each surface increased initially and then decreased

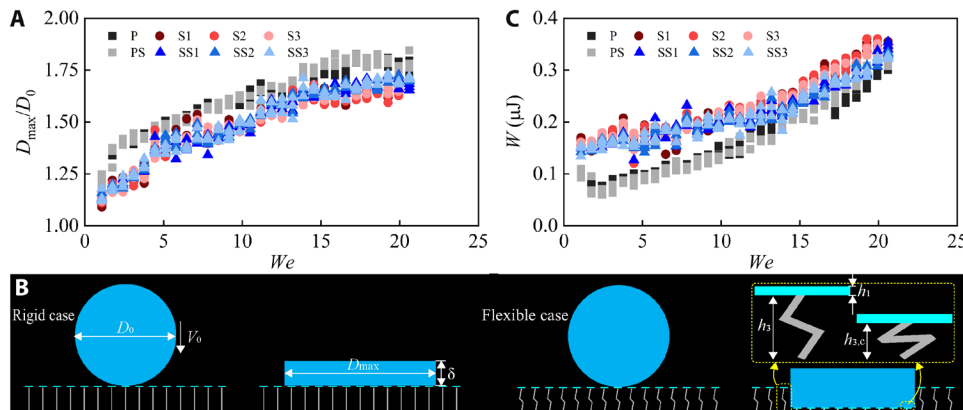


**Fig. 3. Spreading behavior of droplets impacting mushroom-spring and mushroom-pillar surfaces.** (A) Maximum spreading factor  $D_{\max}/D_0$  as a function of  $We$ . (B and C) Theoretical spreading model to estimate the work done  $W$  in spreading phase and the corresponding results as a function of  $We$  (see clear version in figs. S5A and S6A).

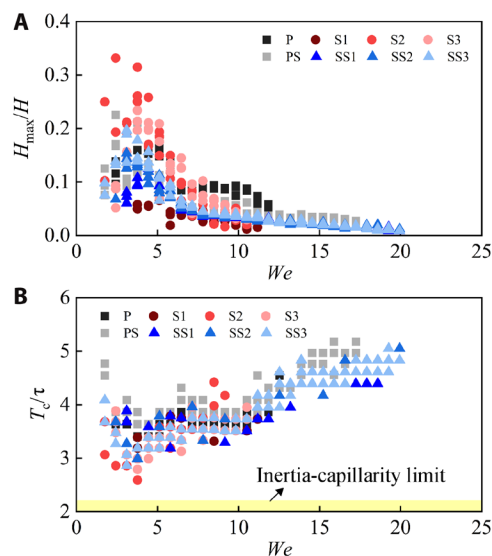


**Fig. 4. Restitution coefficient and contact time of droplets impacting mushroom-spring and mushroom-pillar surfaces.** (A) Restitution coefficient  $H_{max}/H$  as a function of  $We$ . (B) Dimensionless contact time  $T_c/\tau$  as a function of  $We$  and a theoretical inertia-capillarity limit  $T_c/\tau = 2.2$  (see clear version in fig. S5, B and C).

with an increased  $We$ , thus exhibiting a nonmonotonic variation. Because of the various occurrences of the DEP-REB transformation discussed in Fig. 2A, it was difficult to disclose the influence of flexible modification on the restitution coefficient at a low  $We$ . However, when the value of  $We$  was higher than  $\sim 7.81$ , an obvious relationship between the restitution coefficient and structural design can be constructed. Comparing S1, S2, and S3 (or SS1, SS2, and SS3) with P (or PS) showed that the mushroom-spring flexible surfaces exhibited lower restitution coefficients than the corresponding mushroom-pillar rigid surface due to a larger energy consumption when a droplet spread over the flexible surfaces in comparison to the rigid surfaces.

### Contact time

We further discussed the effect of flexible support modification on contact time (see Fig. 4B), which was nondimensionalized by an inertia-capillary time scale  $\tau$  expressed by  $(0.125 \rho D_0^3 / \sigma)^{0.5}$  (34). Most studies have reported a contact time greater than the lowest-order oscillation period of a spherical drop,  $T_c/\tau > 2.2$ , which was sufficiently above the icing time so as to prevent an effective aircraft anti-icing. Since Bird *et al.* in 2013 (35), macro stripes with the aid of micro-nano hierarchical substructures have become a research hot spot due to their effectiveness in reducing the contact time below the theoretical inertia-capillarity limit by splitting impinging droplets (36–38). As the theoretical inertia-capillarity limit relies on a droplet that retracts with a single stationary center and retracting rim, droplet splitting can create additional stationary centers in the retracting phase to reduce the distances between the centers and their corresponding retracting rims, resulting in a measurable reduction in contact time. Of note, the above asymmetric retracting behavior induced by macro stripes arises from different retracting velocities of the droplet on embossed (i.e., macro stripes) and intact regions. However, this type of contact time reduction urges a strict alignment between macro stripes and impinging droplets. As men-

tioned in Introduction, flexible surfaces based on a whole-surface oscillation at impact have found a different way round the problem (19–23). Yet, its contact time reduction is still dependent on the impacting position and has a whole-body oscillation-induced limitation. Our solution is based on the oscillation of flexible microstructures on a rigid substrate and offers an exciting opportunity to overcome the above drawbacks. As depicted in Fig. 4B, our mushroom-spring flexible surfaces indeed reduced contact time in comparison to the mushroom-pillar rigid surfaces while were still above the theoretical inertia-capillarity limit. The confined oscillation space of flexible microstructures has imposed restrictions on the contact time reduction, highlighting a trade-off between the contact time reduction and fabrication efficiency.

### DISCUSSION

In summary, we bridged the gap between two research realms of functional surfaces and mechanical materials implementing a skin-muscle concept in which the top interfacial structures behave as the skin to receive and respond to surrounding stimulus, while the underlying flexible supports function as the muscle to tune mechanical properties. As per this perspective, we designed artificial liquid-repellent surfaces with bioinspired mushroom-like waterproofing heads atop spring-like flexible supports, showing much promise in developing kinetic repellency to liquid intrusion. To resolve the structural instability owing to stress concentration and large aspect ratio, we further proposed an advanced trampoline solution with extra horizontal springs to link adjacent mushroom-like heads. 3D direct laser lithography was used in the micro-nanofabrication to precisely replicate our design. In contrast to the topological optimization of heads in previous works, our design can be of great technological interest because it paves the way for tuning liquid repellency by regulating supports' flexibility. The spring-like flexible supports were proved to contribute a 15.60% improvement of droplet impalement resistance in comparison to conventional rigid supports and even reached a 50.98% enhancement with the aid of trampoline-inspired horizontal springs. Furthermore, the elevation of our flexible supports on kinetic repellency was also exhibited through contact time reduction, which, however, was restricted by confined oscillation space. We believe this study to be the first demonstration of spring-like flexible supports to promote the liquid repellency of mushroom-like interfacial structures, providing an unprecedented level of control over droplet manipulation. Since its beginning, studies on the liquid repellency of interfacial micro/nanostructures have transitioned from conventional statics to dynamics, thus broadening the way of wettability tuning.

Returning to the discussion on impalement resistance and contact time reduction, the confined oscillation space of spring-like flexible microstructures was criticized for its restriction on the frequency relation between flexible microstructures and impinging droplets. At the cost of fabrication efficiency, it is possible to further enlarge the oscillation space by lengthening the free height of spring-like supports, which, however, may introduce new challenges to the trampoline design. Because the allowable amplitudes of oscillation in entire flexible surfaces are higher than  $200 \mu\text{m}$  (19–23), while our repellence enhancement is based on the oscillation of interfacial structures on the microscale, a thorough parametric study is required to determine an optimal height. In addition, although the flexible modification of rigid microstructures can benefit kinetic repellency to impinging droplets,

extreme compliance is also easy to trigger a contact between the droplets and the substrate, thus resulting in a repellency loss (17).

Also noteworthy is that the impalement resistance is not solely determined by flexible supports. Droplet impalement will occur when the pressure arising from impacting events is higher than the breakthrough pressure (12, 17) of mushroom-like heads even if the underlying springs have been compressed to decrease the relative impacting velocity and force. This implies that a droplet impalement can be also triggered by a weak dewetting capacity of mushroom-like heads even with excellent flexible supports, thereby calling for other unprecedented head designs that should be much greater than the up-to-date mushroom-like topology.

Furthermore, in addition to the kinetic repellency elicited by spring-like flexible supports during vertical impact, the flexibility-based enhancement may also endure obliquely impacting droplets (see fig. S9). More precisely, in a mushroom-pillar case, a droplet with an oblique incidence trajectory will impact the heads at an angle, resulting in droplet impalement. While in a mushroom-spring case, the heads can be angularly tuned by the tilting motion of springs to ensure a normal impact with the impinging droplet. We also conducted oblique impacting testes on the fabricated surfaces by tilting the platform through an angle of 45°. No droplet impalement was observed on the rigid surfaces to validate the heroidal assumption above even if  $We$  reached  $\sim 20.61$  (see movie S2). This can be ascribed to the small element pitch  $p$  used on our artificial surfaces, which has been demonstrated as a crucial role in liquid repellency. In addition to the angular flexibility, as an outlook, a further link between functional surfaces and mechanical metamaterials will trigger a window of opportunity for more functionalities and possibilities. For instance, if flexible supports can twist under a normal load (25), then it is possible to gyrate impinging droplets for energy harvesting purposes (39). Of note, although the Nanoscribe direct laser lithography is the most precise rapid prototyping technology to tailor 3D micro-nanostructures, it has to resolve the efficiency problem to realize a large-scale fabrication before daily applications. With the rapid development of 3D printing, more options, e.g., nanoArch, can be used to replicate our mushroom-spring structures in a centimeter-scale fabrication. Moreover, even with a view to mass production, we can use the Nanoscribe system to produce sacrificial photoresist molds, followed by a copy of other materials, e.g., polydimethylsiloxane (40).

## MATERIALS AND METHODS

### Surface fabrication

Using Photonic Professional System (Nanoscribe GmbH, Germany), commercially available IP-S photoresist (Nanoscribe GmbH, Germany) was exposed to a 780-nm femtosecond laser at a speed of  $100 \text{ mm}\cdot\text{s}^{-1}$  with a power of 110 mW. The laser was written 0.5  $\mu\text{m}$  beneath the interface between the photoresist and the ITO-coated fused silica substrate so as to construct a strong adhesion between the structures and the substrate. The resulting fabrication was developed for 20 min in SU-8 Developer (MicroChem Corp., USA) and rinsed in isopropyl alcohol and deionized water.

### Chemical modification

Resulting fabrication was heated in an oven to undergo a chemical vapor deposition of 1H,1H,2H,2H-perfluorooctyltrichlorosilane

at 120°C for 2 hours. Following a natural cooling in the oven, low-surface energy coatings were formed on the fabricated structures.

### Morphology characterization

Morphological images of fabricated surfaces were taken with MXB-2500REZ (Hirox Europe Ltd., France) and S-3400N scanning electron microscope (SEM) (Hitachi Ltd., Japan) accounting for a multiscale requirement.

### Contact angle measurement

Contact angles of 1  $\mu\text{l}$  of water droplets were measured on Ramé-Hart Contact Angle Goniometer (Ramé-Hart Instrument Co., USA) in a sessile drop mode under controlled temperature (20°C) and relative humidity (45%). Each measurement was conducted 30 s after the droplet contacted the target surface for equilibrium. Five measurements were conducted for each target surface for repeatability.

### Droplet impacting test

Spreading, retracting, and post-retraction motions after water droplets impacted the target surfaces were captured in real time by Phantom Miro eX2 (AMETEK Inc., USA) with Zoom 7000 (Navitar Inc., USA) at a rate of 2900 fps. A micro syringe pump was used to release water droplets with a volume of 1  $\mu\text{l}$ . The releasing height was regulated to change the value of Weber number. Three measurements were conducted on each target surface at each specified releasing height.

## SUPPLEMENTARY MATERIALS

Supplementary material for this article is available at <http://advances.sciencemag.org/cgi/content/full/6/32/eaba9721/DC1>

## REFERENCES AND NOTES

1. Y. Lu, S. Sathasivam, J. Song, C. R. Crick, C. J. Carmalt, I. P. Parkin, Robust self-cleaning surfaces that function when exposed to either air or oil. *Science* **347**, 1132–1135 (2015).
2. L. Wang, Q. Gong, S. Zhan, L. Jiang, Y. Zheng, Robust anti-icing performance of a flexible superhydrophobic surface. *Adv. Mater.* **28**, 7729–7735 (2016).
3. H. K. Raut, S. S. Dinachali, Y. C. Loke, R. Ganesan, K. K. Ansah-Antwi, A. Gora, E. H. Khoo, V. A. Ganesh, M. S. M. Saifullah, S. Ramakrishna, Multiscale ommatidial arrays with broadband and omnidirectional antireflection and antifogging properties by sacrificial layer mediated nanoimprinting. *ACS Nano* **9**, 1305–1314 (2015).
4. X. Dai, N. Sun, S. O. Nielsen, B. B. Stogin, J. Wang, S. Yang, T.-S. Wong, Hydrophilic directional slippery rough surfaces for water harvesting. *Sci. Adv.* **4**, eaaq0919 (2018).
5. Q. Sun, D. Wang, Y. Li, J. Zhang, S. Ye, J. Cui, L. Chen, Z. Wang, H.-J. Butt, D. Vollmer, X. Deng, Surface charge printing for programmed droplet transport. *Nat. Mater.* **18**, 936–941 (2019).
6. S. Ben, T. Zhou, H. Ma, J. Yao, Y. Ning, D. Tian, K. Liu, L. Jiang, Multifunctional magnetocontrollable superwetable-microcilia surface for directional droplet manipulation. *Nat. Mater.* **6**, 1900834 (2019).
7. M. Liu, S. Wang, L. Jiang, Nature-inspired superwettability systems. *Nat. Rev. Mater.* **2**, 17036 (2017).
8. R. Hensel, C. Neinhuis, C. Werner, The springtail cuticle as a blueprint for omniphobic surfaces. *Chem. Soc. Rev.* **45**, 323–341 (2016).
9. A. Tuteja, W. Choi, M. Ma, J. M. Mabry, S. A. Mazzella, G. C. Rutledge, G. H. McKinley, R. E. Cohen, Designing superoleophobic surfaces. *Science* **318**, 1618–1622 (2007).
10. A. Tuteja, W. Choi, J. M. Mabry, G. H. McKinley, R. E. Cohen, Robust omniphobic surfaces. *Proc. Natl. Acad. Sci. U.S.A.* **105**, 18200–18205 (2008).
11. R. Hensel, R. Helbig, S. Aland, A. Voigt, C. Neinhuis, C. Werner, Tunable nano-replication to explore the omniphobic characteristics of springtail skin. *NPG Asia Mater.* **5**, e37 (2013).
12. T. Liu, C.-J. Kim, Turning a surface superrepellent even to completely wetting liquids. *Science* **346**, 1096–1100 (2014).
13. R. Hensel, A. Finn, R. Helbig, H.-G. Braun, C. Neinhuis, W.-J. Fischer, C. Werner, Biologically inspired omniphobic surfaces by reverse imprint lithography. *Adv. Mater.* **26**, 2029–2033 (2014).
14. J. H. Kim, T. S. Shim, S.-H. Kim, Lithographic design of overhanging microdisk arrays toward omniphobic surfaces. *Adv. Mater.* **28**, 291–298 (2016).

15. J. Li, Q. H. Qin, A. Shah, R. H. A. Ras, X. Tian, V. Jokinen, Oil droplet self-transportation on oleophobic surfaces. *Sci. Adv.* **2**, e1600148 (2016).
16. G.-T. Yun, W.-B. Jung, M. S. Oh, G. M. Jang, J. Baek, N. I. Kim, S. G. Im, H.-T. Jung, Springtail-inspired superomniphobic surface with extreme pressure resistance. *Sci. Adv.* **4**, eaat4978 (2018).
17. X. Liu, H. Gu, M. Wang, X. Du, B. Gao, A. Elbaz, L. Sun, J. Liao, P. Xiao, Z. Gu, 3D printing of bioinspired liquid superrepellent structures. *Adv. Mater.* **30**, 1800103 (2018).
18. S. Hu, X. Cao, T. Reddyhoff, D. Puhán, S.-C. Vladescu, Q. Wang, X. Shi, Z. Peng, A. J. deMello, D. Dini, Self-compensating liquid-repellent surfaces with stratified morphology. *ACS Appl. Mater. Inter.* **12**, 4174–4182 (2020).
19. T. Vasileiou, J. Gerber, J. Prautzsch, T. M. Schutzius, D. Poulikakos, Superhydrophobicity enhancement through substrate flexibility. *Proc. Natl. Acad. Sci. U.S.A.* **113**, 13307–13312 (2016).
20. P. B. Weisensee, J. Tian, N. Miljkovic, W. P. King, Water droplet impact on elastic superhydrophobic surfaces. *Sci. Rep.* **6**, 30328 (2016).
21. T. Vasileiou, T. M. Schutzius, D. Poulikakos, Imparting icephobicity with substrate flexibility. *Langmuir* **33**, 6708–6718 (2017).
22. J.-H. Kim, J. P. Rothstein, J. K. Shang, Dynamics of a flexible superhydrophobic surface during a drop impact. *Phys. Fluids* **30**, 072102 (2018).
23. P. Chantelot, M. Coux, C. Clanet, D. Quéré, Drop trampoline. *EPL Europhysics Lett.* **124**, 24003 (2018).
24. S. Ushiba, K. Masui, N. Taguchi, T. Hamano, S. Kawata, S. Shoji, Size dependent nanomechanics of coil spring shaped polymer nanowires. *Sci. Rep.* **5**, 17152 (2015).
25. T. Frenzel, M. Kadic, M. Wegener, Three-dimensional mechanical metamaterials with a twist. *Science* **358**, 1072–1074 (2017).
26. O. Tricinci, T. Terencio, B. Mazzolai, N. M. Pugno, F. Greco, V. Mattoli, 3D micropatterned surface inspired by salvinia molesta via direct laser lithography. *ACS Appl. Mater. Inter.* **7**, 25560–25567 (2015).
27. S. Hengsbach, A. D. Lantada, Direct laser writing of fractal surfaces: Strategy to design and manufacture textured materials. *Adv. Eng. Mater.* **17**, 172–180 (2015).
28. E. Davis, Y. Liu, L. Jiang, Y. Lu, S. Ndal, Wetting characteristics of 3-dimensional nanostructured fractal surfaces. *Appl. Surf. Sci.* **392**, 929–935 (2017).
29. A. D. Lantada, S. Hengsbach, K. Bade, Lotus-on-chip: Computer-aided design and 3D direct laser writing of bioinspired surfaces for controlling the wettability of materials and devices. *Bioinspir. Biomim.* **12**, 066004 (2017).
30. S. Hu, X. Cao, T. Reddyhoff, D. Puhán, W. Huang, X. Shi, Z. Peng, D. Dini, Three-dimensional printed surfaces inspired by bi-Gaussian stratified plateaus. *ACS Appl. Mater. Inter.* **11**, 20528–20534 (2019).
31. D. Quéré, Fakir droplets. *Nat. Mater.* **1**, 14–15 (2002).
32. R. Rioboo, M. Voué, H. Adão, J. Conti, A. Vaillant, D. Seveno, J. De Coninck, Drop impact on soft surfaces: Beyond the static contact angles. *Langmuir* **26**, 4873–4879 (2010).
33. D. Soto, A. B. De Larivière, X. Boutillon, C. Clanet, D. Quéré, The force of impacting rain. *Soft Matter* **10**, 4929–4934 (2014).
34. D. Richard, C. Clanet, D. Quéré, Contact time of a bouncing drop. *Nature* **417**, 811 (2002).
35. J. C. Bird, R. Dhiman, H.-M. Kwon, K. K. Varanasi, Reducing the contact time of a bouncing drop. *Nature* **503**, 385–388 (2013).
36. A. Gauthier, S. Symon, C. Clanet, D. Quéré, Water impacting on superhydrophobic macrotextures. *Nat. Commun.* **6**, 8001 (2015).
37. Y. Shen, J. Tao, H. Tao, S. Chen, L. Pan, T. Wang, Approaching the theoretical contact time of a bouncing droplet on the rational macrostructured superhydrophobic surfaces. *Appl. Phys. Lett.* **107**, 111604 (2015).
38. M. Song, Z. Liu, Y. Ma, Z. Dong, Y. Wang, L. Jiang, Reducing the contact time using macro anisotropic superhydrophobic surfaces – effect of parallel wire spacing on the drop impact. *NPG Asia Mater.* **9**, e415 (2017).
39. H. Li, W. Fang, Y. Li, Q. Yang, M. Li, Q. Li, X.-Q. Feng, Y. Song, Spontaneous droplets gyrating via asymmetric self-splitting on heterogeneous surfaces. *Nat. Commun.* **10**, 950 (2019).
40. C. de Marco, C. C. J. Alcántara, S. Kim, F. Briatico, A. Kadioglu, G. de Bernardis, X. Chen, C. Marano, B. J. Nelson, S. Pané, Indirect 3D and 4D printing of soft robotic microstructures. *Adv. Mater. Technol.* **4**, 1900332 (2019).

**Acknowledgments:** We acknowledge the support from the State Key Laboratory of Mechanical System and Vibration in Shanghai Jiao Tong University, the Department of Chemistry and Applied Biosciences in ETH Zurich, and the Department of Mechanical Engineering in Imperial College London. **Funding:** S.H. acknowledges funding support by the China Postdoctoral Science Foundation (2019T120340 and 2017M621458). X.S. acknowledges funding support by the National Natural Science Foundation of China (11572192). Z.P. acknowledges funding support by the National Natural Science Foundation of China (11632011). D.D. acknowledges funding support by the Engineering and Physical Sciences Research Council (EP/N025954/1). **Author contributions:** S.H. designed the study, conducted the test, and wrote the manuscript. X.C. fabricated the surfaces. T.R. provided advice on the experimental investigation and edited the manuscript. D.P. helped with the SEM measurement. S.-C.V. helped with the impacting test. J.W. provided the surface fabrication system. X.S. and Z.P. contributed to the writing of the manuscript. A.J.d. and D.D. edited the manuscript. **Competing interests:** The authors declare that they have no competing interests. **Data and materials availability:** All data needed to evaluate the conclusions in the paper are present in the paper and/or the Supplementary Materials. Additional data related to this paper may be requested from the authors.

Submitted 20 January 2020

Accepted 18 June 2020

Published 5 August 2020

10.1126/sciadv.aba9721

**Citation:** S. Hu, X. Cao, T. Reddyhoff, D. Puhán, S.-C. Vladescu, J. Wang, X. Shi, Z. Peng, A. J. deMello, D. Dini, Liquid repellency enhancement through flexible microstructures. *Sci. Adv.* **6**, eaba9721 (2020).



## Liquid repellency enhancement through flexible microstructures

Songtao Hu, Xiaobao Cao, Tom Reddyhoff, Debashis Puhon, Sorin-Cristian Vladescu, Jing Wang, Xi Shi, Zhike Peng, Andrew J. deMello and Daniele Dini

*Sci Adv* **6** (32), eaba9721.  
DOI: 10.1126/sciadv.aba9721

### ARTICLE TOOLS

<http://advances.sciencemag.org/content/6/32/eaba9721>

### SUPPLEMENTARY MATERIALS

<http://advances.sciencemag.org/content/suppl/2020/08/03/6.32.eaba9721.DC1>

### REFERENCES

This article cites 40 articles, 9 of which you can access for free  
<http://advances.sciencemag.org/content/6/32/eaba9721#BIBL>

### PERMISSIONS

<http://www.sciencemag.org/help/reprints-and-permissions>

Use of this article is subject to the [Terms of Service](#)

---

*Science Advances* (ISSN 2375-2548) is published by the American Association for the Advancement of Science, 1200 New York Avenue NW, Washington, DC 20005. The title *Science Advances* is a registered trademark of AAAS.

Copyright © 2020 The Authors, some rights reserved; exclusive licensee American Association for the Advancement of Science. No claim to original U.S. Government Works. Distributed under a Creative Commons Attribution NonCommercial License 4.0 (CC BY-NC).